An Axisymmetric Coupled Flow and Deformation Model for Pore Pressure Caused by Brine Injection in Paradox Valley, Colorado: Implications for the Mechanisms of Induced Seismicity

Evelyn Roeloffs and Roger Denlinger
U.S. Geological Survey
Vancouver, WA

20 August 2009

This report is preliminary and has not been reviewed for publication.

Executive Summary

We describe a radially-symmetric finite-element model of injectate flow for the Paradox Basin brine disposal well. The model simulates the time variation of the fluid-pressure changes induced by injection as a function of depth below the surface and distance from the wellbore.

The model was calibrated to match the observed wellhead pressure-flow relationship for the period from July 26, 1996 through March 31, 2001. These data provide good constraints on the hydraulic diffusivity of the Leadville injection reservoir in the vicinity of the wellbore, and imply that permeability is 3-4 times lower than the estimate obtained from well logging.

Although the epicenters of the induced earthquakes form linear patterns, the observed pressure-flow behavior is consistent with a radial, rather than a channelized, flow model. If the flow were unable to penetrate uniformly in all directions from the borehole, there would be a much faster fall-off of flow rate with time than observed. However, the observed pressure-flow relationship at the wellbore becomes less sensitive to changes in the permeability structure as distance from the well increases, so a channelized flow pattern developing a few km from the wellhead cannot be ruled out.

The simulated pressure buildup in the Precambrian perforated zone is not as extensive as in the Leadville, but there are still pressure increments in excess of 150 psi 2-3 km from the well in the Precambrian by the end of March, 2001.

Within 4 km of the wellbore, simulated pressure increases of at least 300 psi seem required to induce the first earthquakes. Successive onsets of seismicity occur when the pressure reaches or exceeds its previous maximum.

The first located earthquake more than 3.75 km from the wellhead, on July 26, 1997, seems attributable to elastic stresses acting on a pre-existing fault, rather than to fluid pressure increase at the earthquake's location. The stresses are presumably caused by expansion of the volume around the wellbore as fluid mass is pumped into it. If this interpretation is correct, then this event 7.5 km from the wellbore does not necessarily imply that a fault was providing a preferential flow path or storage reservoir for injectate at that time.

Simulated pressures always decrease monotonically with distance from the well, as does the influence of time-variations in the pumping. Further than 4.75 km from the well, the simulated pressure continues to rise monotonically through March 2001, despite periods during which injection ceases. An important implication, which is probably still true for a more realistic model geometry, is that ceasing injection will not lower fluid pressures at locations several km from the wellbore until months have elapsed.

3D modeling, as well as several geophysical field techniques, could provide independent information to help map the evolving subsurface distribution of injectate.

1. Introduction

We describe a radially symmetric finite element model of injectate flow for the Paradox Basin brine disposal well. The model simulates the time and space distribution of the fluid pressure changes induced by injection versus depth below the surface and distance from the wellbore. We calibrated the model to reproduce the observed pressure-flow relationship at the wellhead based on data through March 2001, and we used the calibrated model to calculate pressure changes in the formation for that time period. These pressure changes can be compared with the temporal and spatial patterns of earthquakes induced by fluid injection. The purpose of this report is to describe the calculated pressure changes and how they relate to earthquakes induced by injection operations.

2. Background

The Paradox Valley injection project was undertaken to dispose of saline groundwater in order to prevent it from entering the Colorado River system. The well is located in the Paradox Valley graben, which overlies a salt-cored anticline near the Colorado/Utah border. The anticline is believed to be controlled by major subsurface faults that displace bedrock beneath the evaporitic Paradox Formation, and the graben is a collapse feature formed by the dissolving of these evaporates (*Widmann, 1997*). The injection well is near the graben-bounding faults southwest of the Valley (Figure 1).

During project planning, in 1984, a network of seismographs was deployed by the U.S. Bureau of Reclamation (BOR) to establish a baseline characterization of natural seismicity in the area prior to beginning injection.

The 4.9 -km-deep injection well was drilled in 1986-1988. It was completed with perforations in the Leadville limestone, in several deeper sandstone units, and in two depth intervals within the deeper Precambrian granite. The perforated zones are overlain by several carbonate units of low permeability as well as by the Paradox salt formation, whose permeability is believed to be negligible. All of the perforations are in the depth range 4.3-4.9 km.

The well was acid- and fracture-stimulated in summer, 1990, and initial injection testing began in July, 1991. The first three injection tests had successively greater maximum flow rates of 150, 225, and 450 gallons per minute (gpm), and each was accompanied by a burst of microseismic activity. The fourth test, at a maximum injection rate of 166 gpm, produced no earthquakes. Prior to the fifth test, the lower Leadville was acid-stimulated. The injection rate during the fifth interval was 300 gpm, and 81 microearthquakes were recorded. During the sixth and seventh injection intervals, flow rates of 300-400 gpm were imposed, and both test intervals were accompanied by bursts of microseismicity. The seventh test interval ended on April 3, 1995.

Injection resumed on a production basis on July 22, 1996 and continued, with some interruptions, at a typical rate of 300-350 gpm and wellhead pressures of about 5000 psi.

Seismicity continued and spread from the immediate vicinity of the borehole. On May 27, 2000 a magnitude 4.3 (MLGs from NEIC) earthquake occurred, whose epicenter was 9 km from the wellhead, and which caused minor damage. Following that earthquake, injection was temporarily stopped, and then resumed at a lower rate.

This study describes a radial model of injectate flow from the well for the purpose of estimating the spatial and temporal pressure distribution caused by the fluid injection. The simulated pressure distribution depends on the permeabilities of the various injection and confining intervals, for which estimates are available from well logging. However, the relationship between the pressure and flow rate at the wellbore is the main piece of information by which to calibrate the simulation, and it will be shown that adjustments to the logging-derived permeabilities are required to simulate the observed relationship. The simulation allows useful statements to be made about the general geometry of the injection zone and the time relationships between pressure changes at the wellhead and pressure changes at the locations where the earthquakes occur.

3. Physical mechanisms by which injection could be inducing earthquakes

There are several distinct physical mechanisms by which fluid injection could be causing earthquakes. Distinguishing among them can be difficult because testing their plausibility requires knowing the pre-existing in-situ state of stress.

Increased fluid pressure reducing effective normal stress across planes of weakness: The Mohr-Coulomb criterion, which is based on laboratory observations of failure and frictional sliding of rock samples, states that shear fracture, or frictional sliding on a pre-existing plane of weakness, occurs when

$$\tau > \tau_0 + \mu(\sigma_n - p) \qquad (1)$$

where τ represents shear stress on the plane, τ_0 represents a shear strength or resistance to frictional failure, μ represents the static friction coefficient (about 0.6 for most crustal rocks) , σ_n is normal stress across the fracture plane (compression positive), and p is pore fluid pressure. Equation (1) predicts that increasing pore fluid pressure can counteract normal stress across the fault plane and lead to shear failure or to sliding. The pore fluid pressure acts in all directions, so increasing fluid pressure destabilizes faults of all orientations.

Hydrofracturing: Extensional cracks in rock can form and propagate when their internal fluid pressure exceeds the normal stress across the crack. Hydrofracturing is a potential mechanism for injection-induced seismicity, especially near the wellbore, where pressure changes of several hundred psi are induced.

Stresses due to pressure gradients: Where fluid pressure gradients are large, a net force on the rock skeleton results, and because this force is spatially nonuniform, it produces stresses. Such stresses are of great importance in the near surface, in unconsolidated materials, but have not been demonstrated to be significant in consolidated rocks at depths of several km.

Elastic stresses due to the increasing volume of injectate. As fluid is pumped into the the wellbore, the surrounding formation expands to accommodate the additional mass. This expansion imposes tensional hoop stresses in the surroundings. These stresses are elastic and therefore can be imposed before the diffusive fluid pressure front arrives at a particular location. Fault slip caused by this mechanism is governed by the Mohr-Coulomb criterion (equation 1), but changes in stress, rather than pore pressure, are the cause of the slip.

The model calculations described here do not assume that any of these mechnisms is the cause of the seismicity at Paradox. The model only calculates the pore pressures, stresses, and displacements, which can then be compared with the spatio-temporal seismicity distribution to infer which of these mechanisms explain the induced seismicity.

4. Description of Model

The model described here is a radially symmetric finite element model with fully coupled poroelasticity (*Ghaboussi and Wilson, 1973*). The complete simulated domain extends from the surface to a depth of 50 km and from the borehole to a radial distance of 50 km, with a refined mesh for depths to 10 km and distances to 20 km. The injection is simulated by applying pressure to nodes at the model borehole wall, following the actual recorded pressure-time history . The model can compute the time-dependent distributions of pore pressure , displacement, stress, strain, and flow throughout the modeled domain. Figure 2 shows a detail of the mesh in the injection interval near the borehole.

5. Physical Properties of the Geologic Units

The model requires specified values for the following physical properties: Shear modulus, Poisson ratio, Skempton coefficient, and hydraulic diffusivity.

The shear modulus strongly affects the size of calculated displacements due to fluid injection; the values assumed in the current model range from 9×10^9 Pa (1.3×10^6 psi) to 2.4×10^{10} Pa (3.5×10^6 psi), with the lower values being used nearer to the surface. All materials in the model are assumed to have a Poisson ratio of 0.25.

Skempton's coefficient is the ratio of pore pressure change to a change of mean stress in a volume of material from which no flow can occur. Theoretically, Skempton's coefficient ranges from 0 to 1. It can be calculated from the porosity and shear modulus. The values used for the porosity and Skempton coefficient are shown in Table 1.

Skempton's coefficient has some effect on the magnitude of the stresses induced by fluid injection.

The hydraulic diffusivity is the parameter that most strongly affects the distribution of pressure in the model. Hydraulic diffusivity is the ratio of transmissivity to storage coefficient, or, equivalently, hydraulic conductivity to storativity, and has dimensions L^2/T. For the model input, diffusivities were calculated from permeabilities, formation thicknesses, porosities, and shear moduli obtained from the BOR and are shown in Table 1.

6. Model Calibration and Sensitivity

The main information available for calibrating the model is the relationship between pressure and flow rate at the wellhead. This relationship in turn is primarily sensitive to the hydraulic diffusivity of the injection interval. Hydraulic diffusivity is directly proportional to permeability, and permeabilities were adusted to obtain the best match to the pressure-flow relationship. However, it should be emphasized that the model actually operates with hydraulic diffusivities, not permeabilities, and that other combinations of permeability, porosity, etc., that yield similar hydraulic diffusivities will produce identical results.

Each material in the injection intervals was assigned a unique hydraulic diffusivity. The pressure-flow relationship at the wellbore is most sensitive to the hydraulic diffusivity of the Leadville formation, because that formation is thickest and most permeable, and therefore takes up most of the fluid. However, since the flow rate represents a total rate into all injection intervals, other combinations of hydraulic diffusivities could fit the observations equally well.

The information provided about the Leadville was that its permeability was "> 100 md". However, it was clear that to successfully reproduce the observed pressure-flow relationship, a permeability 3-4 times lower was required. Figure 3 shows the predicted flow rates for two model runs, together with the actual flow rate history. This figure shows that the permeability of the Leadville is strongly constrained by the data. Overall, the model that assumes a permeability of 28 millidarcies for the Leadville fits the observed flow rates best. The 25% difference between the two permeabilities tested translates to an approximately 25% difference in the simulated flow rate.

Several additional points can be noted from the actual and simulated flow-rate curves in Figure 3:

1. The simulated flow rate gradually decreases with time, but the actual flow rate does not. The behavior of the simulated flow rate is the expected behavior for injection into a medium with uniform, time-independent properties in which the pressure is increasing. The fact that the observed flow rate does not decrease could have several explanations: There could be a zone of higher permeability at some distance from the well; the permeability could be increasing in response to the increase of pore

pressure; or the injectate could be leaking into the confining layers more than the simulation currently permits.

2. The observed pressure-flow behavior is quite consistent with a radial, rather than a channelized, flow model. If the flow were unable to penetrate uniformly in all directions from the borehole, there would be a much faster fall-off of flow rate with time than the simulation. Since the observed flow rate remains above the simulated flow for the radial model, it would not be possible to fit the observations with model in which flow is channelized into a single plane, either vertical or horizontal.
3. Prior to day 120, the simulated flow rate is much higher than the observed flow rate. By day 180, the observed flow rate is consistent with the simulated flow rate. This change in the relationship between the simulated and observed flow rate suggests that the formation permeability may have increased during this time period, or that the flow may have reached a zone of higher permeability away from the well.
4. At about day 640, there is an abrupt increase in injection rate that is not simulated by the model. If this rate is recorded accurately, then this may also represent an episode of fracturing.

7. Simulated Pore Pressure

7.1 Pore pressure vs. distance from well

Figure 4 shows curves of injection-induced pressure versus time at a number of distances from the injection well. At any time, pressure decreases monotonically with distance from the well. The influence of time-variations in the pumping rate also decreases with distance from the well. At distances greater than 4.75 km from the well, the pressure continues to rise monotonically despite periods during which injection ceases.

Figures 5a and 5b show the pressure distribution versus depth and distance from the well 42 days and 1202 days from the beginning of continuous operation. The primary purpose of these figures is to show how the pressure in the Leadville compares with that in the Precambrian. Although the pressure buildup in the Precambrian is not as extensive as in the Leadville, there are still pressure increments in excess of 150 psi 2-3 km from the well in the Precambrian.

7.2 Development of the induced seismicity pattern

In this and the next section, the model-simulated pressure distribution is compared with the time- and space-distribution of earthquakes. The earthquake dataset consists of relative relocations obtained using a 3D velocity model (*L. Block, email communication, file "locs.713.reliable.tec.new", July 2001*). It should be noted that some induced events are not included in this dataset because they could not be located accurately enough. However, it seems likely that this dataset includes the larger events and the improved locations compared with the more complete catalog clarify the relationship of the seismicity to the simulated pressure distribution.

Figure 6 is a map view of the earthquake epicenters color-coded by month for the period from January through October 1997, when the induced seismicity was initially spreading from the well. The first seismicity following the start of production pumping occurred in January, 1997. By the end of April 1997, the induced earthquakes were all less than 1.5 km from the well. On May 5, injection was suspended. On May 5, three events occurred in a cluster about 2.5 km southwest of the wellhead. It may be significant that these events took place as pressure at that location was beginning to decrease following the suspension of injection. No events were located further from the wellhead than this until after the resumption of injection.

Injection was begun again on July 10, 1997. The first induced event after this was on July 16, within the distance range that had remained slightly active during the shutdown. The delay between resuming injection and the onset of seismicity is probably attributable to the time required for the pressure in the formation to exceed its previous maximum, as will be discussed in section 7.3.

The next event, on July 26, took place 7.5 km from the wellhead. This earthquake took place as wellhead pressure was increasing following the resumption of injection. The almost complete lack of any earthquakes between this event and the wellhead strongly suggests that this earthquake was caused by elastic stresses imposed by the increasing amount of mass around the wellbore. Under that interpretation, this earthquake was not an indication that the fluid pressure had suddenly begun propagating more quickly.

The July 26, 1997 earthquake was followed, starting August 5, by activity in a new cluster 2 km west of the wellhead, in which 16 events were located in 10 days. In September, more events took place within about one km of the July 26 earthquake. The distance range between 3 and 6 km from the wellhead remained without activity. A line passing through the epicenters of the July 26 earthquake, the cluster that began August 5, and the September-October activity near the July 26 epicenter is closely parallels the N46° strike of the faults bounding the Paradox Valley graben (*Widmann, 1997*).

Seismicity gradually resumed in the area near the well that had previously been active. Section 7.3 describes how the seismicity at different distances from the wellhead can be related to the simulated pressure changes at those locations.

7.3 Time relationships of pressure and seismicity at increasing distances from well

In each of Figures 7a through 7h, the simulated pressure history at a specific distance from the well is plotted with a timeline of seismicity within an annulus around the same radius.

0.5-1.0 km from the well (Figure 7a). There is a clear relationship between simulated pressure and seismicity. At this distance, every significant drop in the pumping rate modulates the seismicity as well as the simulated pressure. The first earthquake occurs when the simulated pressure is 780 psi. Seismicity rate decreases when the injection pressure decreases and resumes when the simulated pressure reaches 900 psi . Based on

the simulated pressure history, seismicity in this distance range resumes after a period with no pumping when the simulated pressure reaches its previous maximum. As pressure increased steadily from 1050 to 1140 psi, the seismicity rate remained high.

1-1.5 km from the well (Figure 7b). The strongest initial burst of seismicity occurs about 60 days after the first seismicity in the distance range 0.5 to 1 km, when the simulated pressure reaches 620 psi. Seismicity stops as the pressure drops during the temporary cessation of pumping from May 1 to July 10, 1997, and resumes when the simulated pressure reaches 700 psi, about 50 psi above the previous maximum. The simulated pressure then climbs with only one interruption to reach 900 psi in May 1999, and the rate of seismicity also climbs until that maximum is reached. Then the seismicity rate gradually decreases, with some fluctuations that track the simulated pressure. The simulation result is that the 900 psi maximum pressure was not exceeded again before May, 2000.

1.5-2 km from the well (Figure 7c). Seismicity initiates substantially later than the two close intervals discussed previously. The first earthquake occurs at a simulated pressure of about 480 psi. Seismicity ceases when the pressure is dropped, and resumes when the simulated pressure reaches 570 psi, about 100 psi above the previous maximum. As the simulated pressure increases to a maximum of 750 psi, seismicity continues with little modulation by intervals of low injection pressure. At this distance from the wellhead, temporary drops in wellhead pressure cause smaller and more gradual decreases in simulated pressure.

2-2.5 km from the well (Figure 7d). Two events occurred when simulated pressure reached 390 psi, and then no more activity took place until after injection resumed. The next seismicity is the cluster of events starting August 5 (Figure 6), which begins at a simulated pressure of about 310 psi. Unlike earlier onsets nearer the borehole, this cluster began when the simulated pressure was 100 psi lower than the previously simulated maximum. As will be discussed in Figure 7h, this cluster is likely related to the July 26, 1997 event 7.5 km from the wellbore. The next two onsets of seismicity follow the pattern of occurring at, or slightly above, the previous maximum simulated pressure. Sustained activity occurs as the simulated pressure rises to its maximum of 650 psi, and then activity decreases and stops as the pressure is maintained below that value. As at the closer distances to the borehole, events occur at lower simulated pressures after the M4.3 earthquake in May 1997. At this distance there is a significant delay in the response of the simulated pressure to periods when injection is temporarily stopped.

2.5 to 3 km from the well (Figure 7e). The first seismicity occurred when the simulated pressure was 320 psi, and subsequent onsets occur at or above the previous maximum simulated pressure. Periods when injection is stopped cause small, gradual pressure decreases, but these variations do still appear to influence the seismicity rate.

3-3.5 km from the well (Figure 7f). Activity does not initiate here until early 1998, but the simulated pressure at onset (380 psi) is not very different from that for the 2.5-3 km range (320 psi). Earthquakes occur less frequently than closer to the wellbore, and the

simulation indicates that brief interruptions in injection produce only small changes in pressure, so it is not clear whether the pressure variations modulate the seismicity. The seismicity rate can be seen in Figures 7a through 7f to have decreased with increasing distance from the wellbore, consistent with decreasing injection-induced pressures.

3.5-6 km from the well (Figure 7g). Only one earthquake occurred during the simulated time period, at a distance of 3.75 km from the wellhead. The simulated pressure rises almost monotonically, and the earthquake occurred at a simulated pressure of 310 psi, not very different from the onset pressures at distances of 2.5-3.5 km. The maximum pressure is 360 psi and it is maintained for the 10-month period from the May 27 M4.3 earthquake to the end of the figure, despite the cessation of pumping.

6-9 km from the well (Figure 7h). Activity more than 6 km from the well began with the event on July 26, 1997 7.5 km from the wellhead. This event could be interpreted to indicate that the fluid pressure there had increased sufficiently to induce an earthquake. However, the pattern of response to the simulated pressure observed closer to the wellbore does not support that interpretation. First, it is implausible that the fluid pressure due to injection would be greater at this distance than in the 3.5-6 km distance range, where no earthquakes occurred before 1998. Second, the event occurred when the simulated pressure was only 60 psi, whereas pressures in excess of 300 psi were simulated when seismicity closer to the wellhead began. Third, although this event occurred only 16 days after injection had resumed, the simulated pressure was simply climbing monotonically, owing to the large distance to the wellhead, and therefore provides no obvious trigger for the event to occur.

An alternative explanation is that the earthquake 6 km away on July 26 was caused by slip on a pre-existing fault to help accommodate the increasing volume of material being added around the wellbore. If the pressurized material around the borehole is regarded as cylindrical, then extensional hoop stresses intensify as more material is injected, reducing the normal stress across pre-existing subvertical faults. Such stress increments are elastic responses to increased pressurization near the wellbore and they are therefore imposed on the same time scale as that pressurization. The rapidly increasing pressure near the wellbore as injection resumed after a break (Figures 7a thru 7c) would have imposed rapidly changing stresses on the surrounding region. It is plausible that these stresses led to the earthquake on July 26, by causing a critical effective stress to be reached, and/or because of the rapid nature of the change.

7.4 Summary of relationship between seismicity and simulated pressure

Although the distribution of seismicity is not radial, this radially symmetric model seems to account for some specific features in the data.

Within 4 km of the wellbore, when the onset times of seismicity at various distances from the borehole are compared with the simulated pressure at that distance, successive onsets of seismicity can be seen to occur when the pressure reaches its previous maximum.

All of the earthquakes in this dataset that occurred within 4 km of the wellbore took place when the simulated injection-induced pressure was 300 psi or more.

During the time period of this simulation (from July 22, 1996 to March 31, 2001), simulated pressure at the initiation of seismicity decreases with distance from the wellbore (from 780 psi within 1 km of the wellbore, to about 300 psi at 3 km from the wellbore). This could be explained in several ways. First, if injectate is confined to a narrower reservoir, actual pressures would not decrease with distance as quickly, so the lower simulated pressures further from the wellbore could be due to inappropriateness of the radial model. Second, during the period of development and testing prior to production, the formation near the wellbore presumably experienced higher maximum pressures, so that the simulation period may not include the first onset of seismicity for locations nearest the well. It is of course possible that stresses are higher, or faults are less resistant to slip, at distances several km from the wellbore, but this hypothesis is difficult to test.

The first located event more than 3.75 km from the wellhead, on July 26, 1997, seems attributable to elastic stresses acting on a pre-existing fault, rather than to fluid pressure increase at the earthquake's location. The stresses are presumably caused by expansion of the volume around the wellbore as fluid mass is pumped into it. This earthquake was followed by seismic events (on August 5, 1997) closer to the wellbore along the strike of regional faults. However, this alignment of earthquakes does not necessarily imply that a fault was providing a preferential flow path or storage reservoir for injectate in the time period shown here.

Figures 7a through 7h illustrate how pressure variations at the wellhead are damped out with increasing distance from the well. An important implication is that ceasing injection will not lower fluid pressures at locations several km from the wellbore until months have elapsed. This general conclusion would also be true in a situation where flow is confined to a narrow region.

8. Suggestions for future work

Further modeling, ideally supplemented by field measurements, could provide constraints on where the Paradox injectate is flowing in the subsurface. Because increased fluid pressure is not necessarily the cause of the induced earthquakes more than a few km from the wellhead, it could be misleading to identify the pressure front with the expansion of the seismically active area. Independent means of mapping the fluid distribution are needed.

Modeling needs to be undertaken with a 3D code that can evaluate the possibility that flow is channelized and that can more accurately represent the geologic structure in the area.

Seismological techniques for detecting velocity changes may help map the distribution of subsurface pressure. Focal mechanisms for the earthquakes would help discriminate among the various possible mechanisms for inducing seismicity at Paradox. This preliminary study suggests that increases of pore pressure alone cause earthquakes within a limited radius of the well, while stresses imposed by addition of so much fluid mass can induce earthquakes on pre-existing faults further from the wellbore.

Crustal deformation measurements using leveling, tiltmeters, or borehole strainmeters could help ascertain the influence of the injected fluid on the earth's crust. All three techniques would be useful within a few km of the wellhead. Borehole strainmeters might well detect strains associated with injection at the distances of 10 km or more where events are potentially migrating. Boreholes are also excellent low-noise environments for seismometers that could record low-level activity outside the perimeter of the existing network.

References Cited

Ghaboussi, J. and E. L. Wilson, Flow of compressible fluid in a porous elastic medium with compressible constituents, *International Journal of Numerical Methods in Engineering*, **5**, 419-442, 1973.

Widmann, B.L., compiler, 1997, Fault number 2286, Paradox Valley graben, in Quaternary fault and fold database of the United States: U.S. Geological Survey website, http://earthquakes.usgs.gov/regional/qfaults, accessed 08/19/2009 07:44 PM.

Figure captions

Figure 1. Map showing location of the injection well and the surrounding area.

Figure 2. Cross-section diagram of the finite element mesh used for a radially symmetric simulation of pore pressure and deformation at the Paradox Salinity Control Injection Well. Complete mesh extends to the surface and to 50 km in the radial and depth directions.

Figure 3. Actual injection pressure history, and model-simulated pressure histories for two different assumed permeabilities of the Leadville formation.

Figure 4. Model-simulated injection-induced pressure as a function of time at a number of distances from the injection well.

Figure 5. Cross-section views of the model-simulated injection-induced pressure distribution for two elapsed times after injection resumed on a production basis on July 22, 1996. (a) 42 days after July 22, 1996. (b) 1202 days after July 22, 1996.

Figure 6. Map view of earthquake epicenters (*3D locations from L. Block, email communication*) for January through October, 1997.

Figure 7. Simulated pressures and timelines of earthquakes for several distance ranges from the injection well.

Table Caption.

Table 1. Physical properties used in the finite-element model.

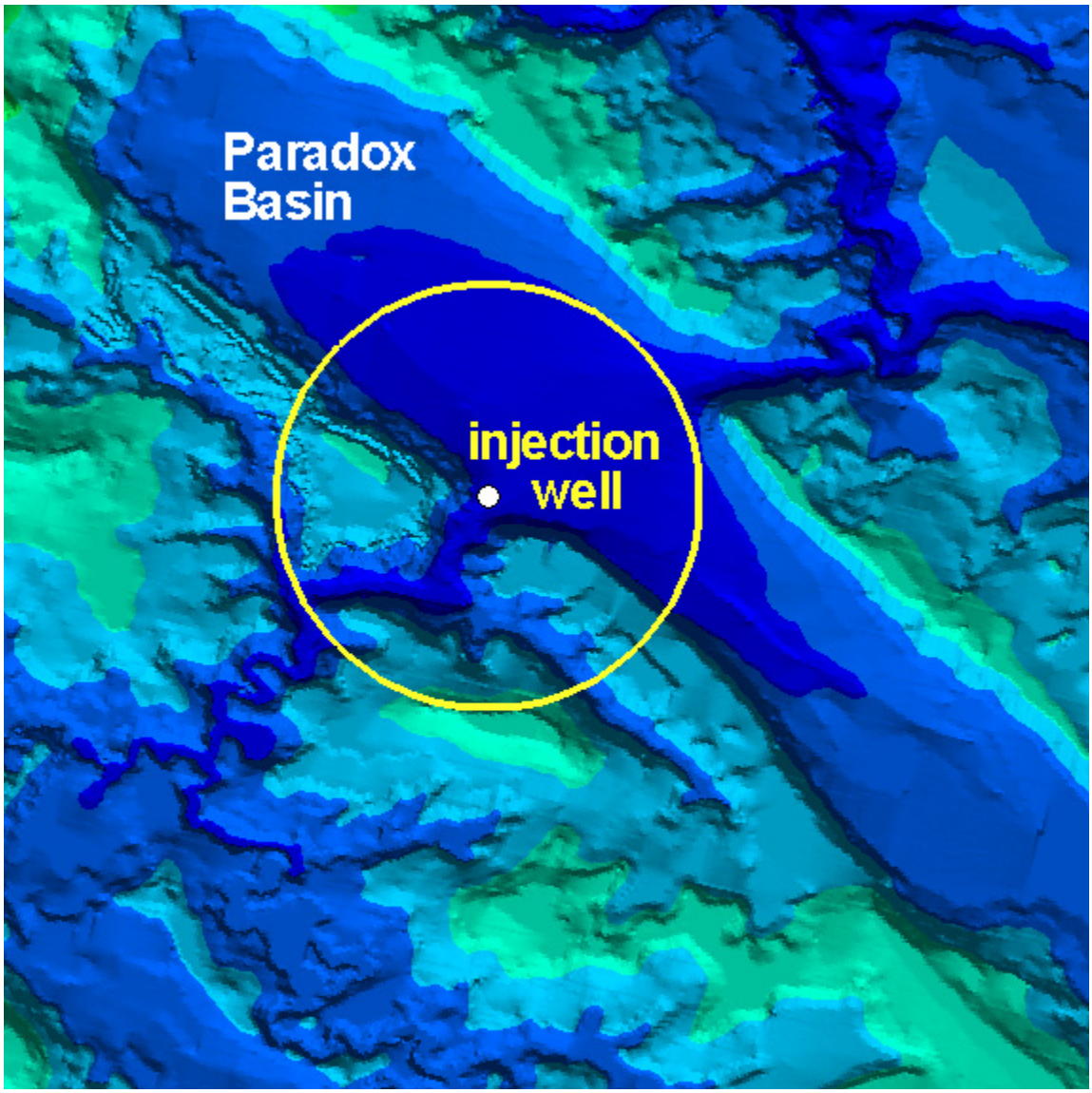

FIGURE 1

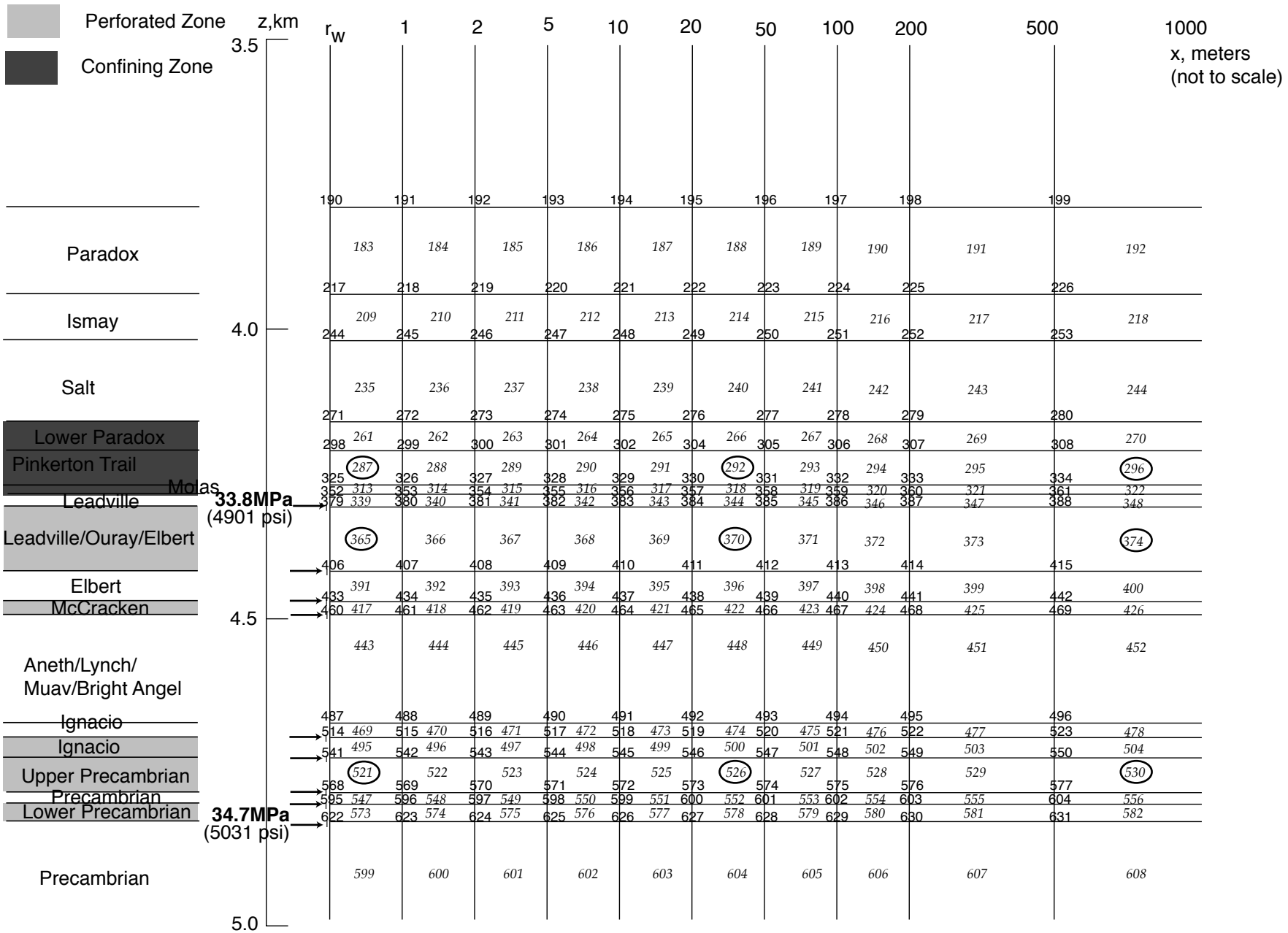

FIGURE 2

Figure 1. Detail of finite element mesh used for a radially symmetric simulation of pore pressure and deformation at the Paradox Salinity Control Injection Well. Complete mesh extends to the surface and to 50 km in the radial and depth directions.

Paradox Very Small Mesh

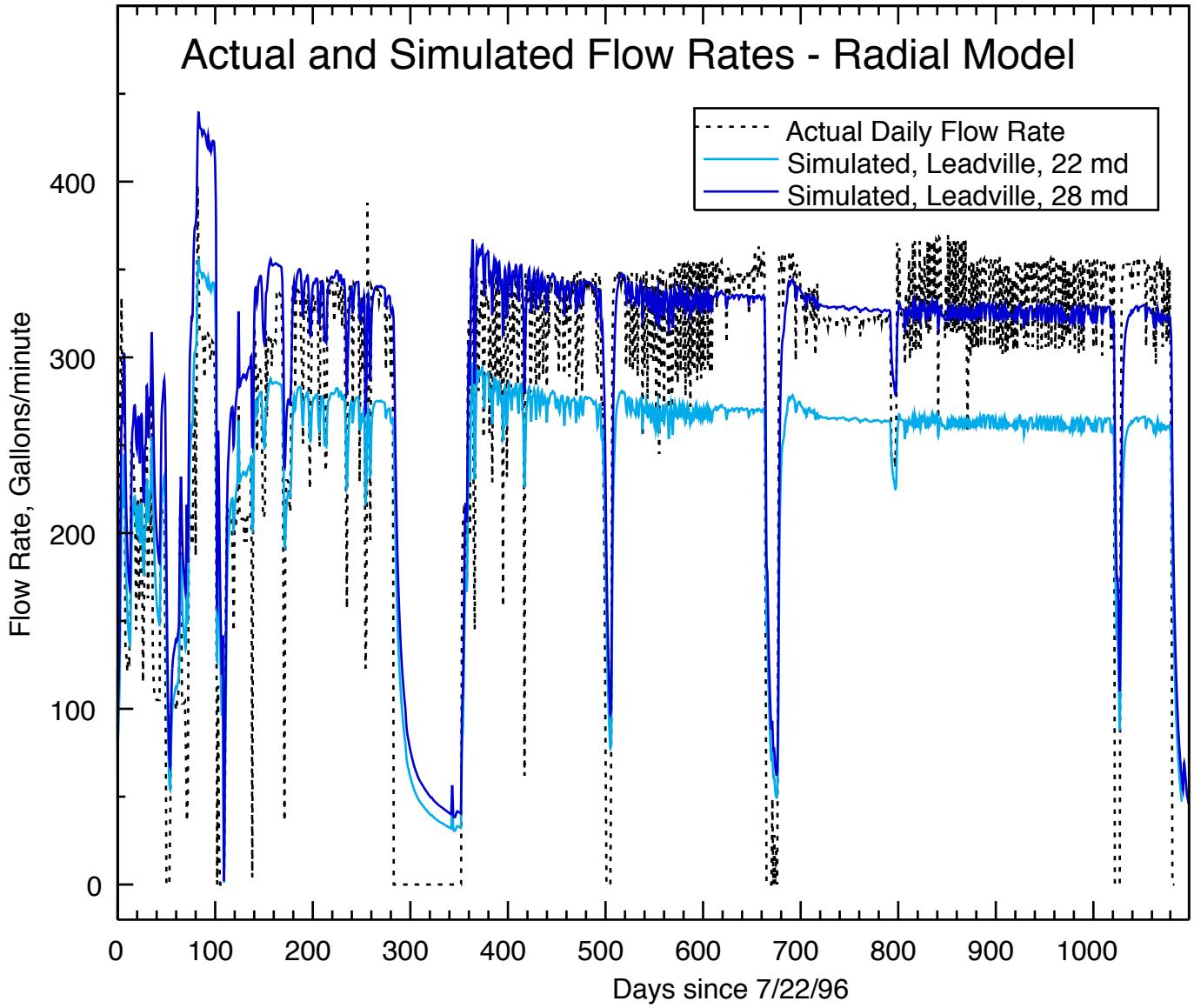
Actual and Simulated Flow Rates - Radial Model
Actual Daily Flow Rate
Simulated, Leadville, 22 md
Simulated, Leadville, 28 md
Flow Rate, Gallons/minute
0
100
200
300
400
0
100
200
300
400
500
600
700
800
900
1000
Days since 7/22/96

FIGURE 3

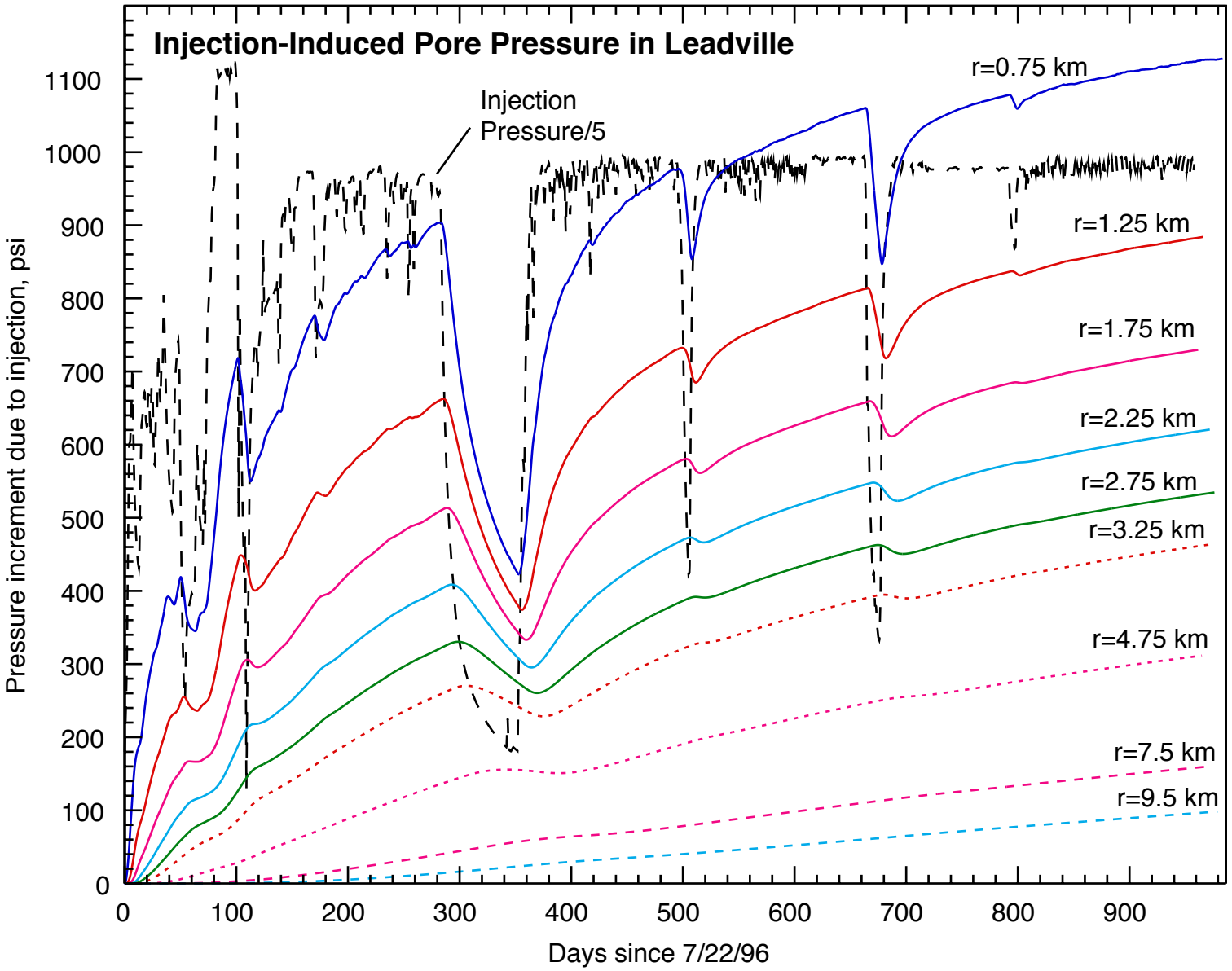
Injection-Induced Pore Pressure in Leadville
Injection
Pressure/5
r=0.75 km
r=1.25 km
r=1.75 km
r=2.25 km
r=2.75 km
r=3.25 km
r=4.75 km
r=7.5 km
r=9.5 km
Pressure increment due to injection, psi
Days since 7/22/96
0
100
200
300
400
500
600
700
800
900
1000
1100

FIGURE 4

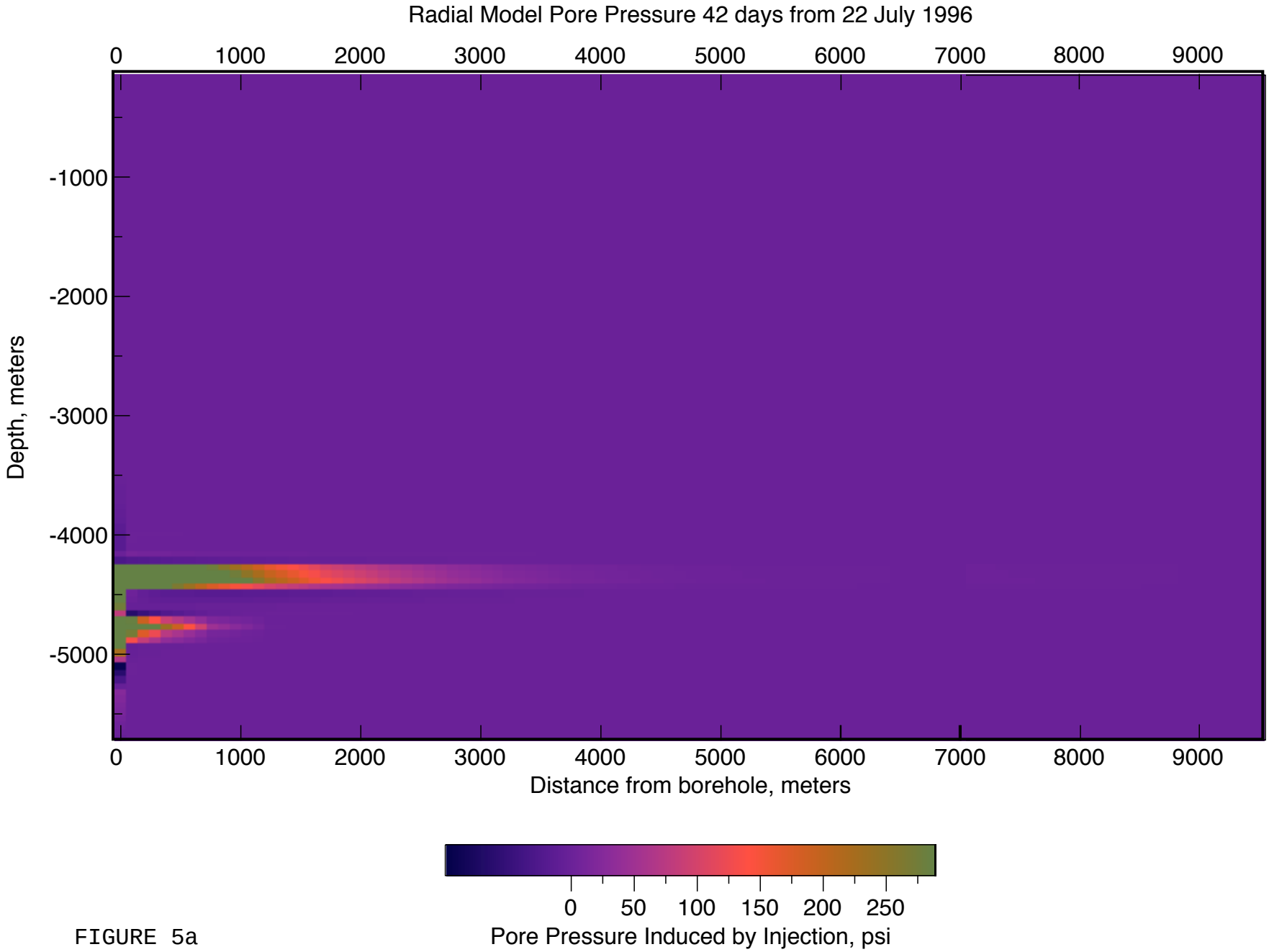
Radial Model Pore Pressure 42 days from 22 July 1996
0
1000
2000
3000
4000
5000
6000
7000
8000
9000
-1000
-2000
-3000
-4000
-5000
Depth, meters
Distance from borehole, meters
0
50
100
150
200
250
Pore Pressure Induced by Injection, psi

FIGURE 5a

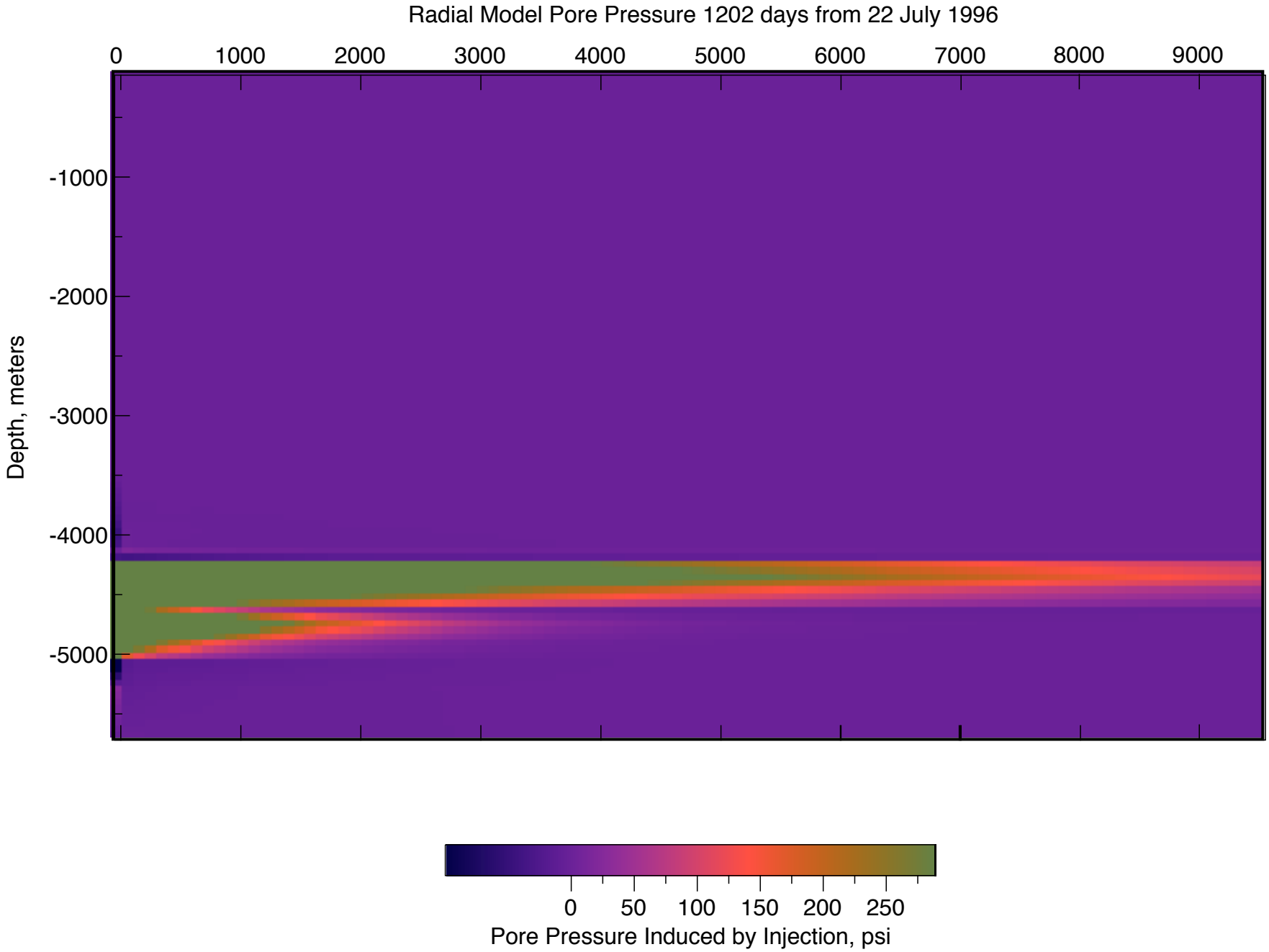
Radial Model Pore Pressure 1202 days from 22 July 1996
0
1000
2000
3000
4000
5000
6000
7000
8000
9000
-1000
-2000
-3000
-4000
-5000
Depth, meters
0
50
100
150
200
250
Pore Pressure Induced by Injection, psi

FIGURE 5b

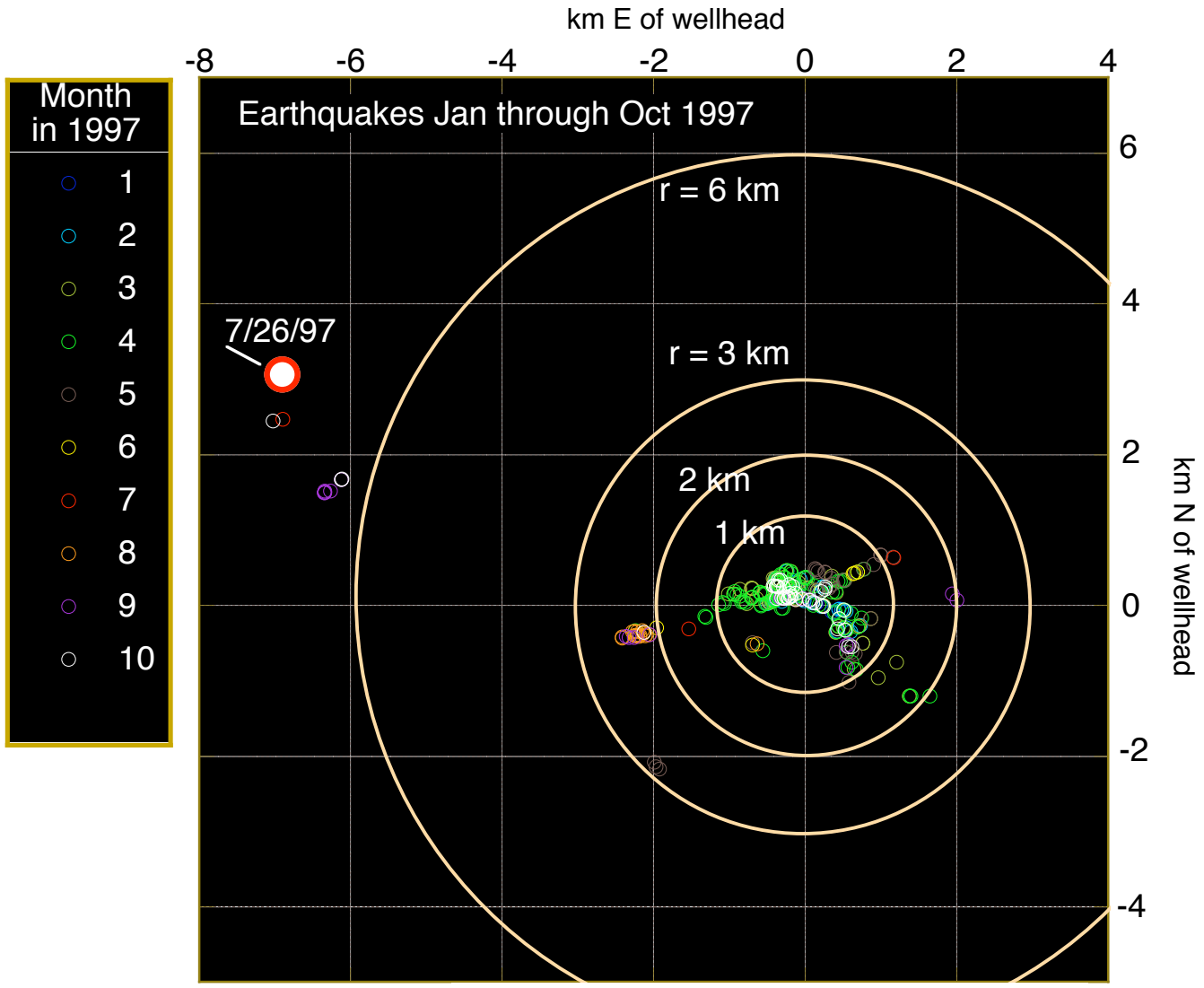

FIGURE 6

locs.713.tec.a kgdata

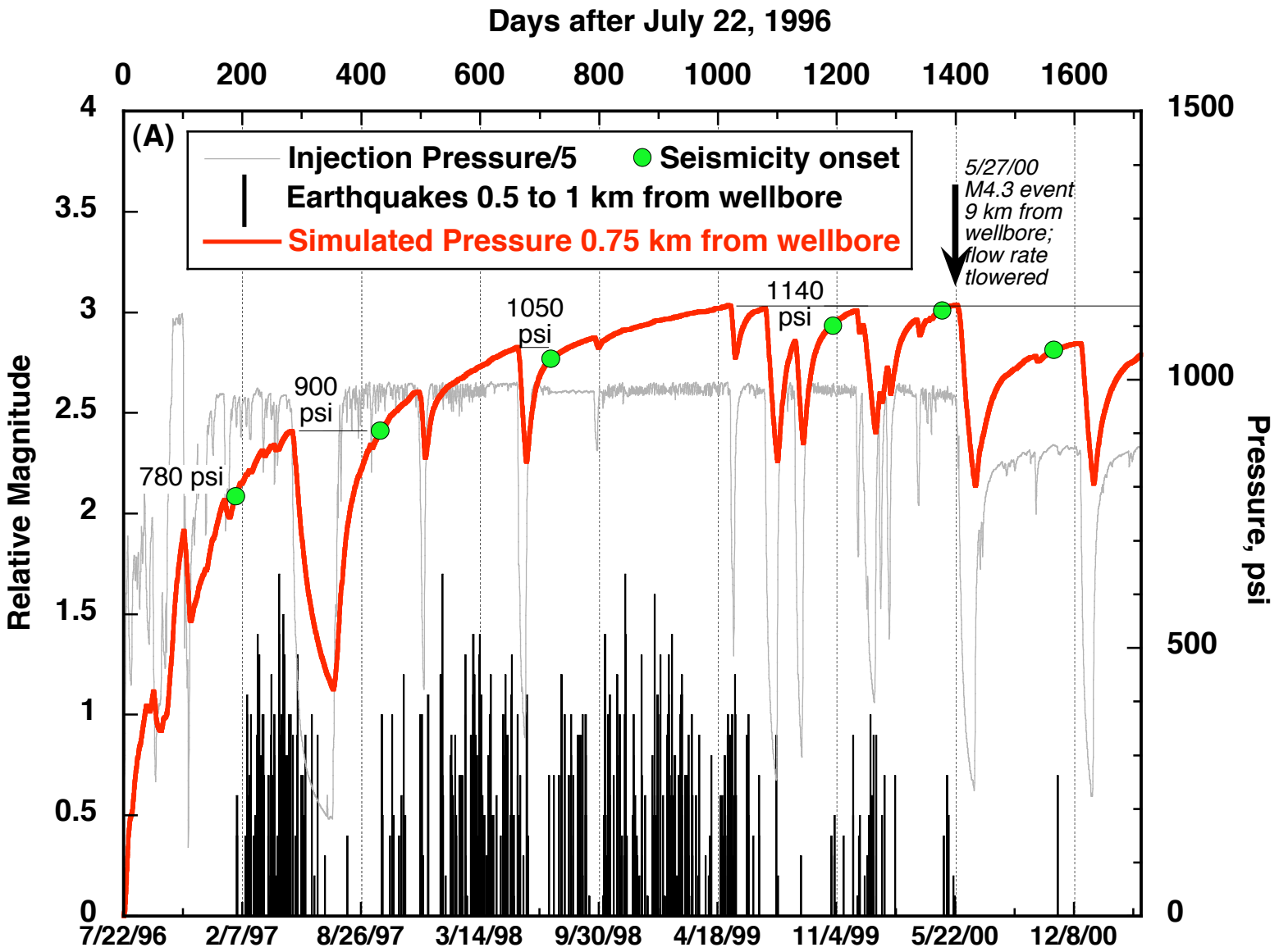
Days after July 22, 1996
0
200
400
600
800
1000
1200
1400
1600
(A)
Injection Pressure/5
Seismicity onset
Earthquakes 0.5 to 1 km from wellbore
Simulated Pressure 0.75 km from wellbore
5/27/00
M4.3 event
9 km from
wellbore;
flow rate
tlowered
780 psi
900
psi
1050
psi
1140
psi
Relative Magnitude
Pressure, psi
4
3.5
3
2.5
2
1.5
1
0.5
0
1500
1000
500
0
7/22/96
2/7/97
8/26/97
3/14/98
9/30/98
4/18/99
11/4/99
5/22/00
12/8/00

FIGURE 7a

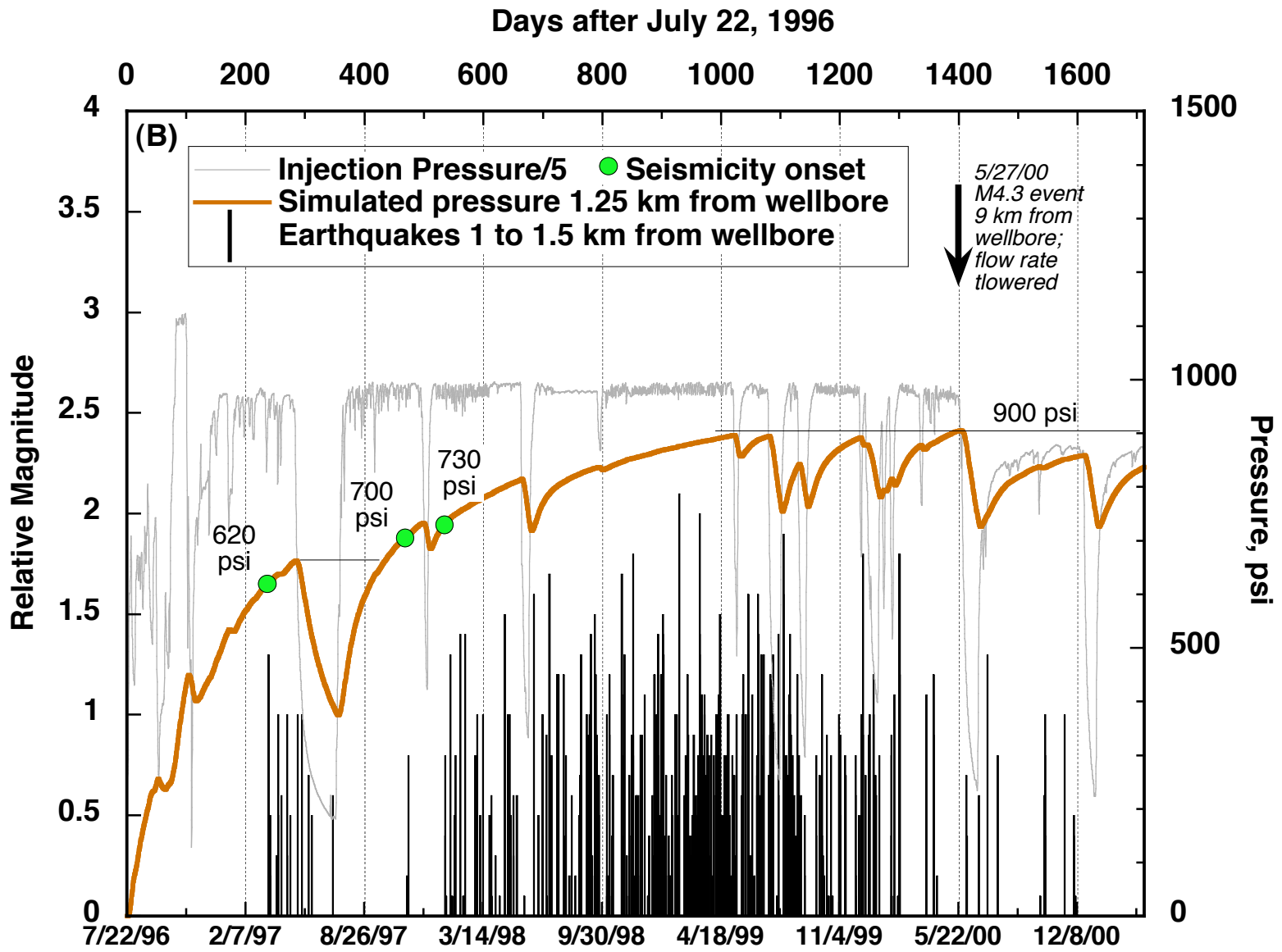
Days after July 22, 1996
0
200
400
600
800
1000
1200
1400
1600
(B)
Injection Pressure/5
Seismicity onset
Simulated pressure 1.25 km from wellbore
Earthquakes 1 to 1.5 km from wellbore
5/27/00
M4.3 event
9 km from
wellbore;
flow rate
tlowered
900 psi
730
psi
700
psi
620
psi
Relative Magnitude
Pressure, psi
4
3.5
3
2.5
2
1.5
1
0.5
0
1500
1000
500
0
7/22/96
2/7/97
8/26/97
3/14/98
9/30/98
4/18/99
11/4/99
5/22/00
12/8/00

FIGURE 7b

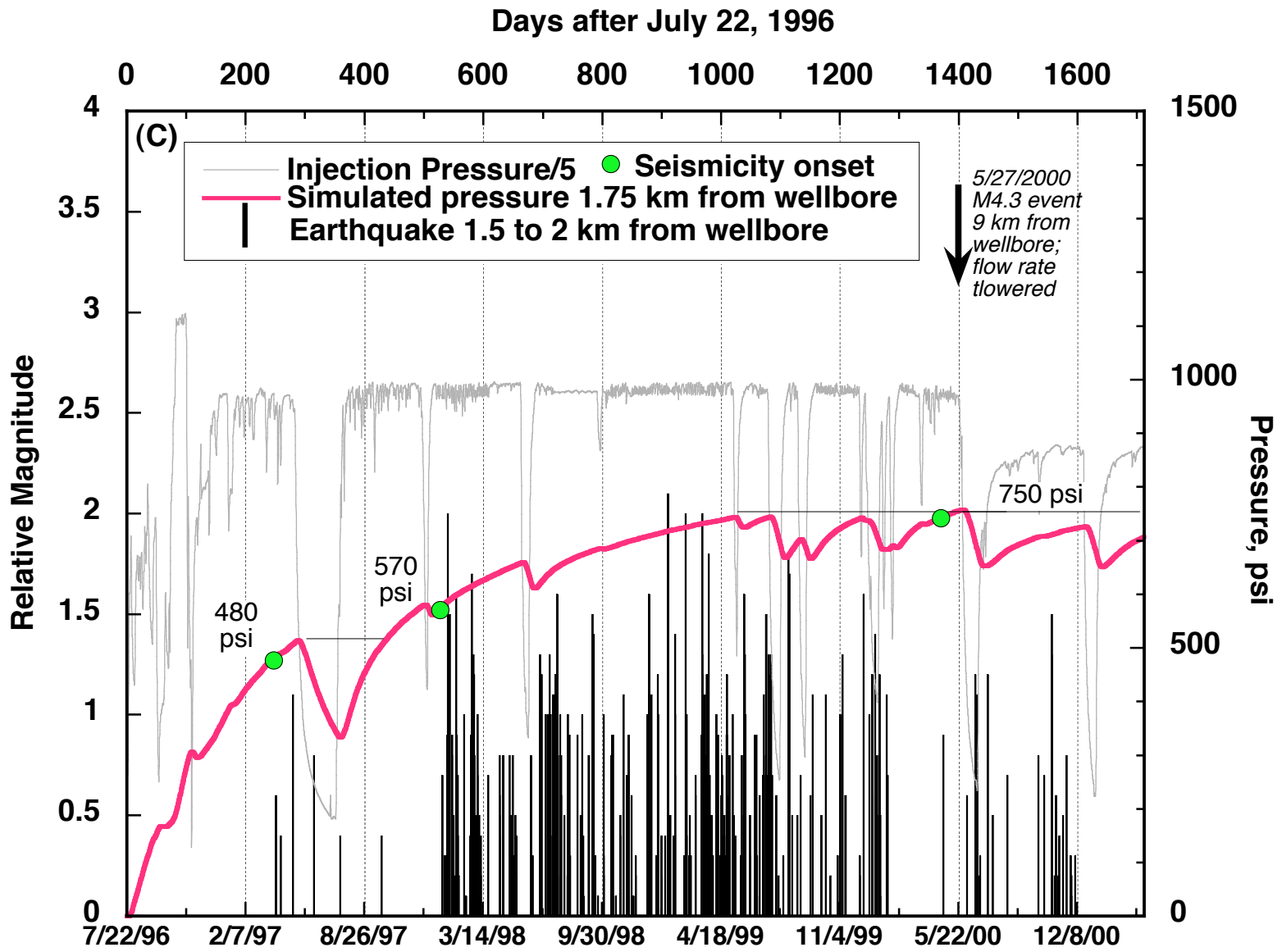
Days after July 22, 1996
0
200
400
600
800
1000
1200
1400
1600
(C)
Injection Pressure/5
Seismicity onset
Simulated pressure 1.75 km from wellbore
Earthquake 1.5 to 2 km from wellbore
5/27/2000
M4.3 event
9 km from
wellbore;
flow rate
tlowered
480
psi
570
psi
750 psi
Relative Magnitude
Pressure, psi
4
3.5
3
2.5
2
1.5
1
0.5
0
1500
1000
500
0
7/22/96
2/7/97
8/26/97
3/14/98
9/30/98
4/18/99
11/4/99
5/22/00
12/8/00

FIGURE 7c

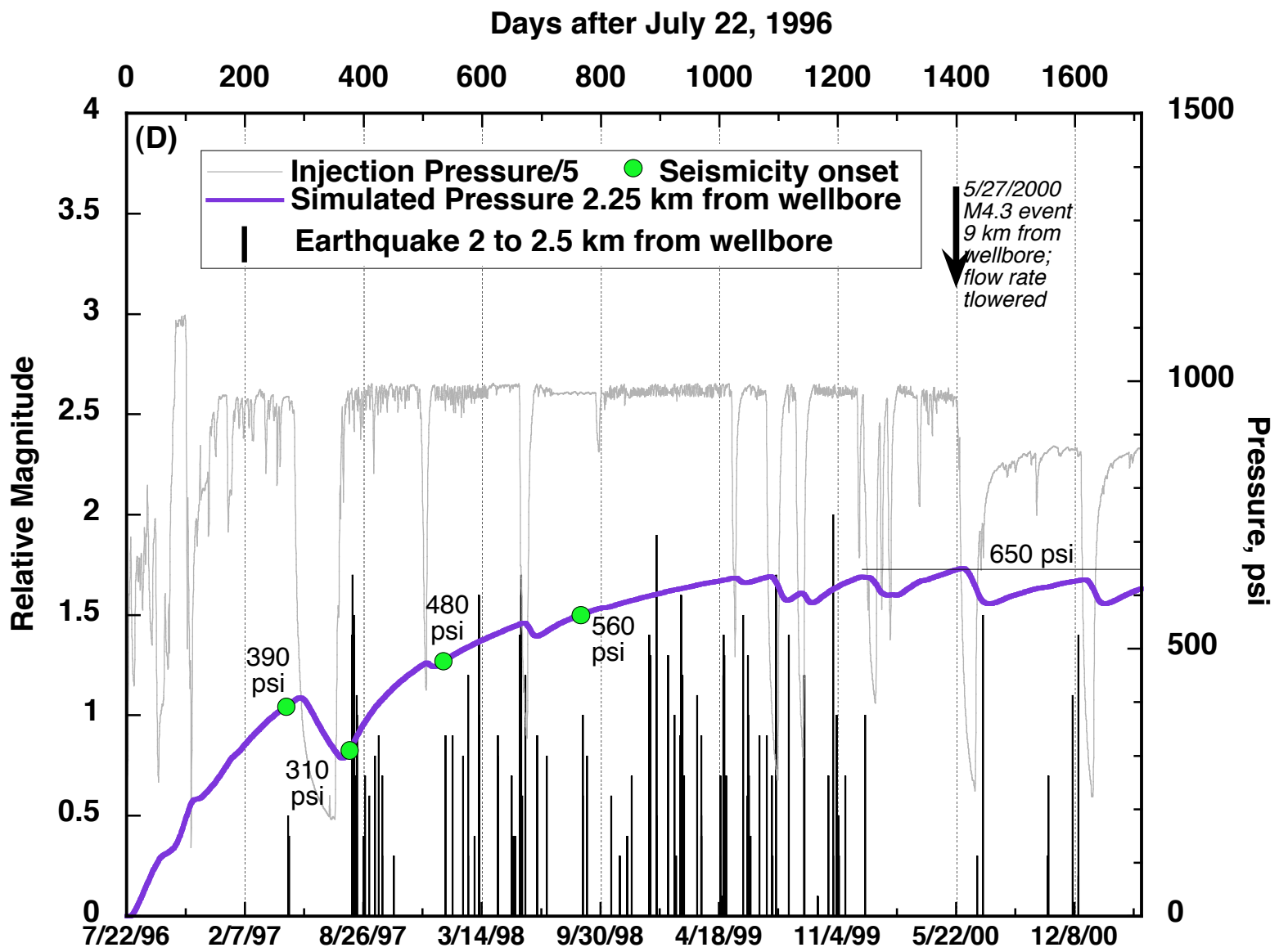
Days after July 22, 1996
0
200
400
600
800
1000
1200
1400
1600
(D)
Injection Pressure/5
Seismicity onset
Simulated Pressure 2.25 km from wellbore
Earthquake 2 to 2.5 km from wellbore
5/27/2000 M4.3 event 9 km from wellbore; flow rate tlowered
650 psi
390 psi
310 psi
480 psi
560 psi
Relative Magnitude
Pressure, psi
4
3.5
3
2.5
2
1.5
1
0.5
0
1500
1000
500
0
7/22/96
2/7/97
8/26/97
3/14/98
9/30/98
4/18/99
11/4/99
5/22/00
12/8/00

FIGURE 7d

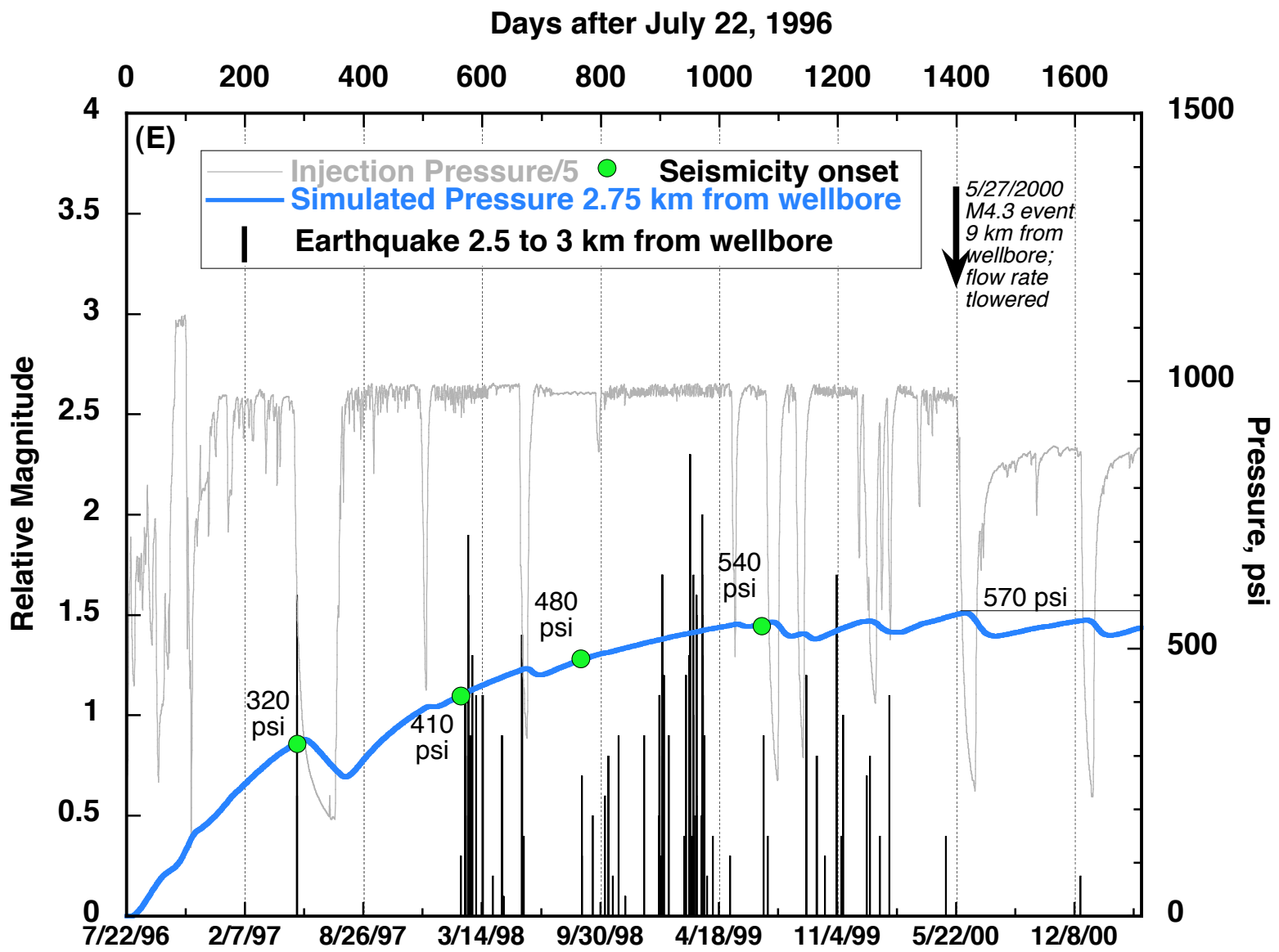
Days after July 22, 1996
0
200
400
600
800
1000
1200
1400
1600
(E)
Injection Pressure/5
Seismicity onset
Simulated Pressure 2.75 km from wellbore
Earthquake 2.5 to 3 km from wellbore
5/27/2000
M4.3 event
9 km from
wellbore;
flow rate
tlowered
320
psi
410
psi
480
psi
540
psi
570 psi
Relative Magnitude
Pressure, psi
4
3.5
3
2.5
2
1.5
1
0.5
0
1500
1000
500
0
7/22/96
2/7/97
8/26/97
3/14/98
9/30/98
4/18/99
11/4/99
5/22/00
12/8/00

FIGURE 7e

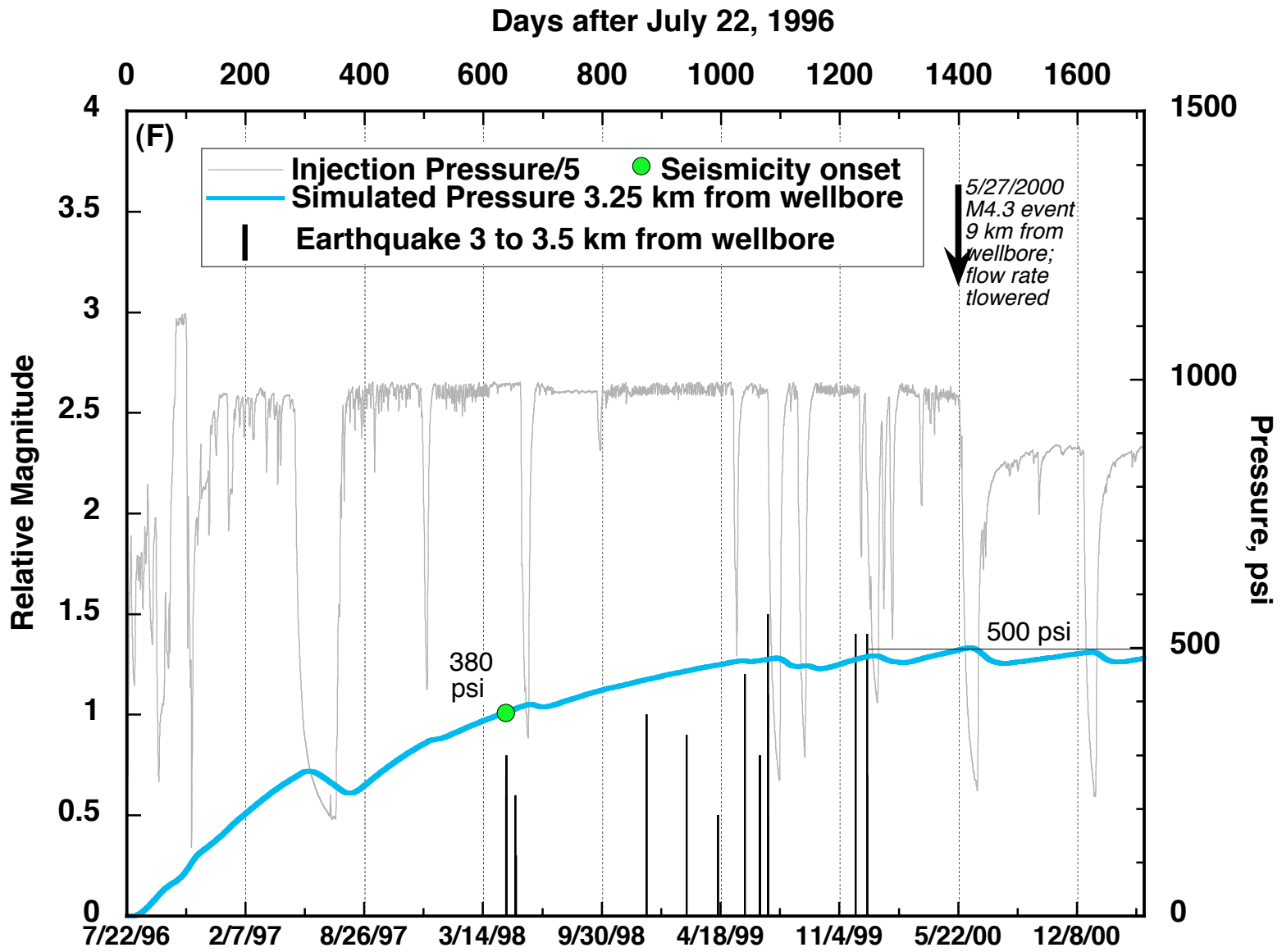
Days after July 22, 1996
0
200
400
600
800
1000
1200
1400
1600
(F)
Injection Pressure/5
Seismicity onset
Simulated Pressure 3.25 km from wellbore
Earthquake 3 to 3.5 km from wellbore
5/27/2000
M4.3 event
9 km from
wellbore;
flow rate
tlowered
380
psi
500 psi
Relative Magnitude
Pressure, psi
4
3.5
3
2.5
2
1.5
1
0.5
0
1500
1000
500
0
7/22/96
2/7/97
8/26/97
3/14/98
9/30/98
4/18/99
11/4/99
5/22/00
12/8/00

FIGURE 7f

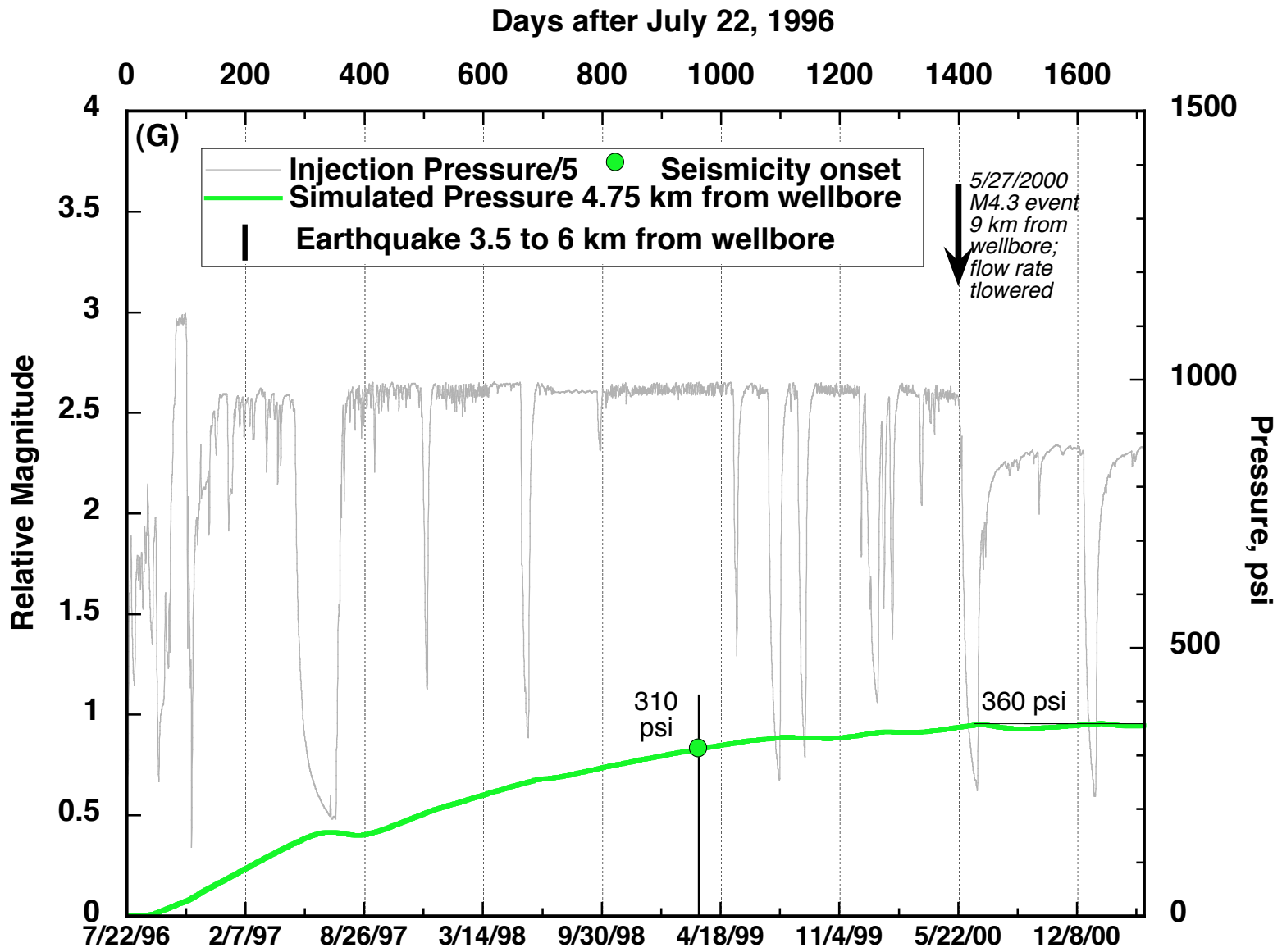
Days after July 22, 1996
0
200
400
600
800
1000
1200
1400
1600
(G)
Injection Pressure/5
Seismicity onset
Simulated Pressure 4.75 km from wellbore
Earthquake 3.5 to 6 km from wellbore
5/27/2000
M4.3 event
9 km from
wellbore;
flow rate
tlowered
Relative Magnitude
Pressure, psi
4
3.5
3
2.5
2
1.5
1
0.5
0
1500
1000
500
0
310
psi
360 psi
7/22/96
2/7/97
8/26/97
3/14/98
9/30/98
4/18/99
11/4/99
5/22/00
12/8/00

FIUGRE 7g

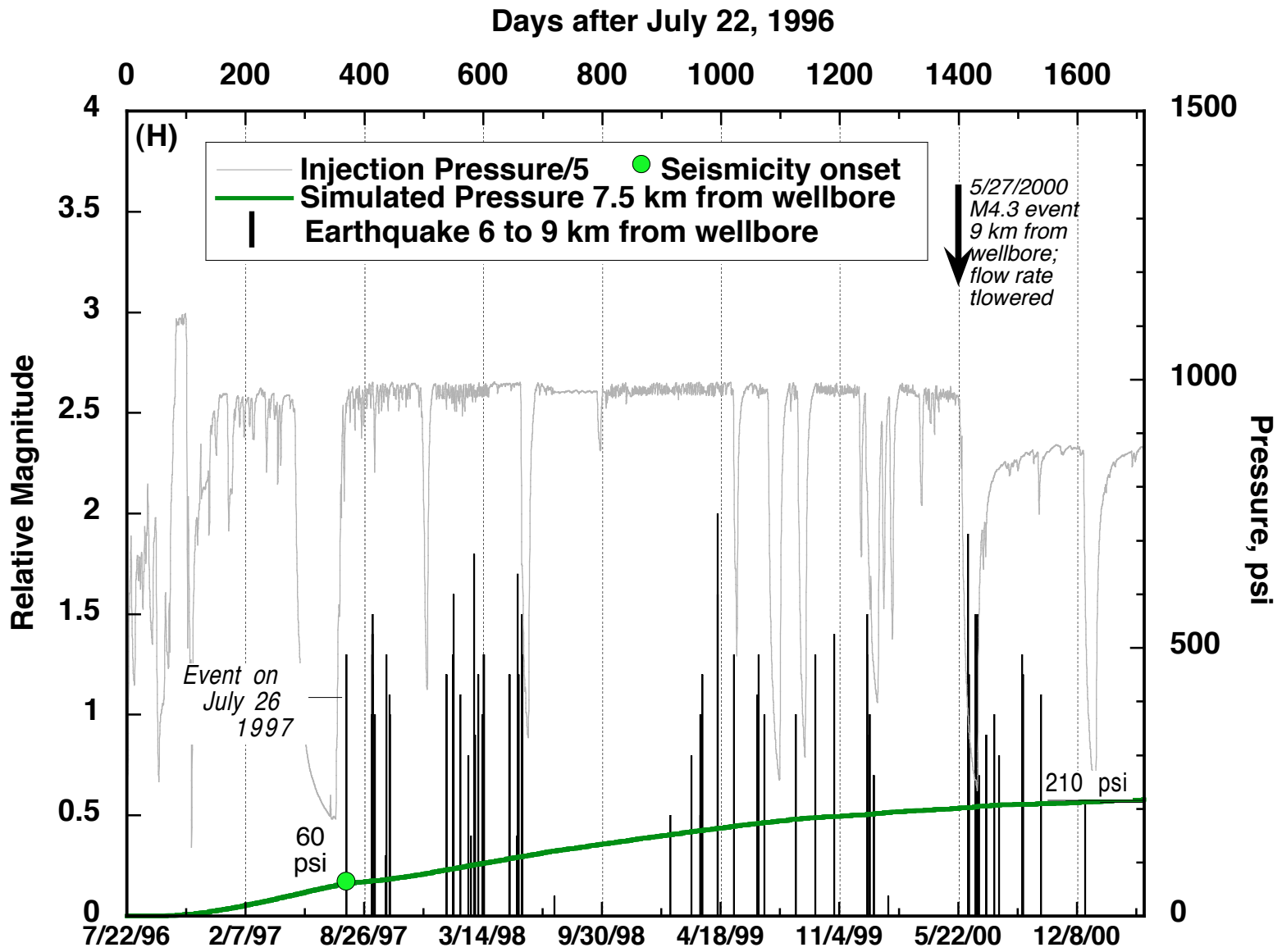
Days after July 22, 1996
0
200
400
600
800
1000
1200
1400
1600
(H)
Injection Pressure/5
Seismicity onset
Simulated Pressure 7.5 km from wellbore
Earthquake 6 to 9 km from wellbore
5/27/2000
M4.3 event
9 km from
wellbore;
flow rate
tlowered
Relative Magnitude
Pressure, psi
4
3.5
3
2.5
2
1.5
1
0.5
0
1500
1000
500
0
Event on
July 26
1997
60
psi
210 psi
7/22/96
2/7/97
8/26/97
3/14/98
9/30/98
4/18/99
11/4/99
5/22/00
12/8/00

FIGURE 7h

	Information from Fact Sheet					Model Input			
Formation	Description	Top (m KB)	Thickness (m)	Porosity	K, darcies	K,millidarcies, in simulation	Porosity	Skempton's Coefficient	Hydraulic Diffusivity, m**2/sec
Chinle		0	347			1.00E+01	0.1	0.61	1.68E-01
Cutler		347	2192			1.00E+01	0.1	0.61	1.68E-01
Honaker Trail		2539	1236			1.00E+01	0.1	0.61	1.68E-01
Paradox	Salt and anhydrite	3775	149		low	1.00E-08	0.0001	1.00	4.75E-10
Ismay		3923	82			1.00E-08	0.0001	1.00	4.75E-10
Salt		4005	142			1.00E-08	0.0001	1.00	4.75E-10
Lower Paradox	Carbonate	4147	38		"tight"	1.00E-06	0.001	0.98	6.82E-08
Pinkerton Trail	Carbonate	4185	77		"impervious"	1.00E-06	0.001	0.98	6.82E-08
Molas	Limestone or shale?	4262	12		"impervious"	1.00E-06	0.001	0.98	6.82E-08
Leadville (unperf)	Limestone, oolitic, fossiliferous	4275	17	>0.1	>100 md	2.79E+01	0.1	0.39	6.56E-01
Leadville/Ouray/Elb Perf		4292	129			2.79E+01	0.1	0.39	6.56E-01
Elbert (unperf)		4414	51			2.79E-03	0.05	0.56	9.80E-05
McCracken (almost all perforated)	Sandstone	4465	23			2.79E-03	0.05	0.56	9.80E-05
Aneth-Lynch-Muav-Bright Angel	Limestone with Sandstone	4487	173			2.79E-03	0.05	0.56	9.80E-05
Ignacio (unperforated)	Sandstone	4660	27			2.79E-04	0.05	0.56	9.80E-06
Ignacio (perforated)	Sandstone	4687	34	0.04-0.07	no data	2.79E-04	0.05	0.56	9.80E-06
Upper Precambrian Perf Zone	Granite	4721	58	0.03-0.09	3.2 md	8.36E-01	0.06	0.15	4.25E-02
Precambrian (unperf?)	Granite	4779	21			2.79E-04	0.005	0.68	6.60E-05
Lower Precambrian Perf Zone	Granite	4801	30			2.79E-04	0.005	0.68	6.60E-05
Precambrian						2.79E-04	0.005	0.68	6.60E-05

TABLE 1